# Multi-Channel ScanSAR for High-Resolution Ultra-Wide-Swath Imaging

Nicolas Gebert, Gerhard Krieger, and Alberto Moreira
German Aerospace Center (DLR), 82234 Wessling, Germany

## Abstract

**Multi-channel radar systems allow for overcoming the inherent limitation of conventional synthetic aperture radar (SAR). An example is the combination of digital beamforming on receive in elevation with multi-aperture SAR signal reconstruction in azimuth which enables high-resolution wide-swath imaging [1]. As a next step, focus is turned to advanced concepts for the imaging of even wider swaths with high azimuth resolution [2]. In this regard, the paper investigates the operation of multi-channel SAR systems in burst modes like ScanSAR or TOPS-SAR and analyses aspects of applying the multi-aperture reconstruction algorithm in combination with burst mode operation. The impact of the digital processing network on the *SNR* and the azimuth ambiguity-to-signal-ratio in multi-channel burst mode systems ($AASR_{N,B}$) are considered and embedded in the design example of a ScanSAR system that enables the imaging of a 400 km wide swath with a geometric resolution of 5 m.**

## 1. Introduction

### 1.1 High-Resolution Wide-Swath Imaging by Multi-channel SAR

Multi-channel SAR systems gather additional information with their multiple receive apertures what enables to image wide swaths with a high geometric resolution (cf. Fig. 1). As discussed in [1], such systems require additional signal processing by a suitable digital beamforming algorithm to cope with spatially non-uniformly sampled data in azimuth resulting from *PRFs* that deviate from the optimum value given in (1) , where $v_s$ is the sensor velocity, $N$ the number of adjacent sub-apertures and $\Delta x$ the size of a single sub-aperture.

$$PRF_{uni} = \frac{2 \cdot v_s}{N \cdot \Delta x} \qquad (1)$$

A solution to the digital beamforming problem is given by the multi-aperture reconstruction algorithm, that is based on an unambiguous recovery of the aliased azimuth spectrum by applying for a given *PRF* to each of the system's channels $j$ a Doppler frequency $f$ dependent filter function $P_{j,PRF}(f)$.

As shown in [1], a possible degradation of the *SNR* caused by the inverse character of the filters $P_{j,PRF}(f)$ has to be considered. This is described by $\Phi_{bf}$ that quantifies the decrease of the *SNR* due to the digital beamforming network (cf. (2)).

$$\Phi_{bf}(PRF) := \frac{p_{n,el} \cdot \sum_{j=1}^{N} \mathrm{E}\left[\left|P_{j,PRF}(f)\right|^2 \cdot rect\left(f/B_D\right)\right]}{N \cdot \mathrm{E}\left[\left|U(f) \cdot rect\left(f/B_D\right)\right|^2\right]} \qquad (2)$$

It takes into account the focusing with a Doppler bandwidth $B_D$ that is expressed by $rect(f/B_D)$ representing a rectangular window function of width $B_D$. Noise and signal power, respectively, are defined by the mean value on the frequency band $[-N \cdot PRF/2,\ N \cdot PRF/2]$ what is denoted by the operator **E[.]**. The signal power is governed by the normalized SAR signal $U(f)$ that corresponds to the signal envelope if a "white" scene is assumed while the noise power is given in dependency on the input noise power $p_{n,el}$ and scaled by the filter functions $P_{j,PRF}$. As $\Phi_{bf}$ rises with increasing deviation from $PRF_{uni}$, (2) finally restricts the *PRF* range of operation. This can be mitigated or overcome by various optimization strategies presented in [1].

Similar to the *SNR*, the digital beamforming by the fil-

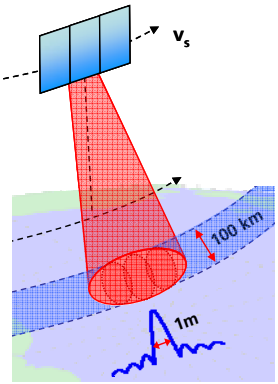


**Fig. 1. High-Resolution Wide-Swath SAR System.**

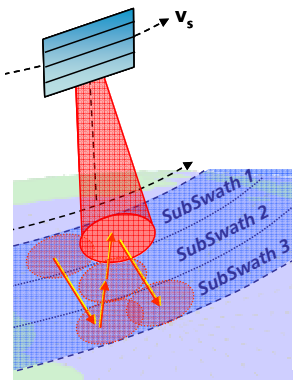


**Fig. 2. Burst Mode System (ScanSAR).**

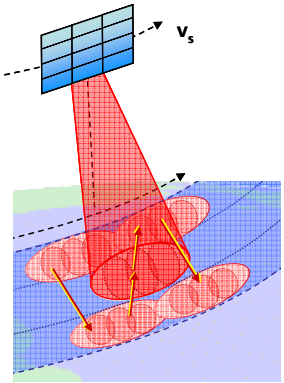


**Fig. 3. Multi-Aperture System in Burst Mode Operation.**

ters $P_{j,PRF}(f)$ also has to be taken into account to determine the azimuth-ambiguity-to-signal ratio in multi-channel systems denoted by $AASR_N$ (cf. (3)). $U_k(f)$ represents the *k-th* continuation of the signal spectrum after sampling while $H_{jk}(f)$ basically represents the two-way channel of transmitter and receiver *j*. The index *k* again indicates a frequency shift by $k \cdot PRF$ due to the periodic continuation by sampling and index *m* specifies one of the *N* sub-bands of the Doppler spectrum that make up the system bandwidth.

$$AASR_N(PRF) = \frac{\mathrm{E}\left[\left|2 \cdot \sum_{k=1}^{\infty}\left(U_k(f) \cdot \sum_{m=1}^{N}\sum_{j=1}^{N} H_{jk}(f) \cdot P_{jm,PRF}(f)\right) \cdot rect\left(\frac{f}{B_D}\right)\right|^2\right]}{N^2 \cdot \mathrm{E}\left[\left|U(f) \cdot rect\left(\frac{f}{B_D}\right)\right|^2\right]} \quad (3)$$

### 1.2 Burst Mode Operation

In burst mode operation like ScanSAR [3][4] or TOPSAR [5] the antenna footprint is switched continuously between a number of sub-swaths, what allows for an overall swath width that consists of all sub-swaths but is at the cost of a reduced illumination time per sub-swath entailing a coarsened azimuth resolution (cf. Fig. 2). The necessary illumination time, $T_B$, or Doppler bandwidth, $B_B$, respectively, of a single burst to obtain an azimuth resolution $\delta_{az}$ is given as follows, where $R_0$ gives the mean slant range distance and $\lambda$ the carrier wavelength.

$$T_B = \frac{\lambda \cdot R_0}{2 \cdot 0.89 \cdot v_s^2} B_B \approx \frac{\lambda \cdot R_0}{2 \cdot v_s \cdot \delta_{az}} \quad (4)$$

Taking into account the number of necessary bursts, $N_B$, the cycle time $T_C$ is determined by the left equality of (5). In addition, the equality on the right of (5) ensures that each target is continuously illuminated for the time $T_B$ while located within the antenna footprint defined by the angle $\Theta_a$.

$$T_C = N_B \cdot T_B = \frac{R_0 \cdot \Theta_a}{v_s} - T_B \quad (5)$$

From equation (5) follows the overall bandwidth $B_D$ in azimuth.

$$B_D = (N_B + 1) \cdot B_B \quad (6)$$

## 2. Multi-channel SAR in Burst Mode Operation

### 2.1 Basic Considerations

As discussed in [1], future multi-aperture SAR systems with a reasonable antenna length of 11.2 m enable a swath of 100 km with a resolution of 1 m in stripmap mode. In a next step the advantages of multi-aperture systems operated in burst modes are investigated in order to allow for ultra-wide swaths of several hundreds of kilometres with a resolution well below 10 m (cf. Fig. 3). In this context a multi-channel ScanSAR system design example will be given in Section 3 where the intricate connection between multi-aperture system design and the various parameters becomes clear. Especially the impact of the variable target position within the burst that results in a variable Doppler band of the reflected signal will be investigated with respect to the Doppler frequency dependent multi-aperture processing network. To provide a consistent notation in the following, the target position within the burst will be "translated" to a "target center frequency" denoted $f_{c,t}$ that represents the mean frequency of the Doppler spectrum reflected by the target.

### 2.2 Azimuth-Ambiguity-to-Signal Ratio: $AASR_{N,B}$

As mentioned in Section 1.1 and derived in detail in [1], the residual azimuth ambiguities in the SAR image are governed by the aliasing contributions in the originally received signal in combination with a possible amplification due to the weighting by the reconstruction filter functions $P_{j,PRF}(f)$ of the digital beamforming network (cf. (3)). Further, this weighting is frequency dependent, resulting in an amplification that depends on the Doppler band where the ambiguous contribution is situated. Consequently, as the target signal spectrum depends on the target's position relative to the burst, the ambiguous power will vary with this target position.

In the following, two scenarios are considered. Firstly, a single burst is processed to obtain the SAR image. The resulting spectrum $B_{s,1}$ (cf. (7)) is characterized by a bandwidth $B_B$ around a varying center frequency $f_{c,t}$ corresponding to the signal position.

$$B_{s,1} = \left[f_{c,t} - \frac{B_B}{2}, f_{c,t} + \frac{B_B}{2}\right] \quad (7)$$

Secondly, additionally the second burst situated – partly - within the band $B_D$ is processed and the results for both bursts are added incoherently. In this case, an additional signal band $B_{s,2}$ has to be considered that can be obtained from the "main" burst $B_{s,1}$ shifted by a frequency $f_{off,B}$ corresponding to the time $T_C$ between the two bursts (cf. (8)). The limitation to components within $B_D$ is expressed by the operator '$\cap$'.

$$B_{s,2} = \left[f_{c,t} - \frac{B_B}{2} - f_{off,B}, f_{c,t} + \frac{B_B}{2} - f_{off,B}\right] \cap B_D \quad (8)$$

This allows for modifying (3) to obtain $AASR_{N,B}$ in (9) that quantifies the azimuth ambiguous energy suppression in burst mode operation. The functions $W(B_{s,i})$ indicate rectangular windows confining the respective band. If both $B_{s,i}$ are considered, the respective signal powers given by the denominator and noise powers defined by the numerator of (9) are to be added separately. The ratio of the sums then yields the $AASR_{N,B}$.

$$AASR_{N,B,i} = \frac{\mathrm{E}\left[\left|2 \cdot \sum_{k=1}^{\infty}\left(U_k(f) \cdot \sum_{m=1}^{N}\sum_{j=1}^{N} H_{jk}(f) \cdot P_{jm,PRF}(f)\right) \cdot W(B_{s,i})\right|^2\right]}{N^2 \cdot \mathrm{E}\left[\left|U(f) \cdot W(B_{s,i})\right|^2\right]} \quad (9)$$

Hence, besides the well-known varying signal power ('scalloping'), the use of different sub-spectra corresponding to different target positions within the burst will result in a large variation of the residual azimuth ambiguities of these targets thus yielding a scalloping-like effect for the $AASR_{N,B}$ as it varies with $f_{c,t}$ as can be seen in Fig. 7. Note that also in TOPS SAR mode the scaling will vary depending on the target position. Nevertheless the variations are expected to be smaller

than in ScanSAR due to the constant signal power ensured by the TOPS mode.

### 2.3 *SNR* Scaling: $\Phi_{bf,B}$

The resulting *SNR* depends on the applied focusing method. If the complete system bandwidth $B_D$ is focused at once, all spectral noise components within $B_D$ are considered and consequently the possible rise of the noise power due to the beamforming network is not affected by the Doppler band of the respective target. In this case the numerator of expression (2) is valid to quantify the noise scaling, but one has to include the well-known scalloping, i.e. the variation of the signal power with $f_{c,t}$ in the denominator (cf. (10)). In contrast, if multiple sub-bands of the Doppler band are focused separately and the image is obtained by combining the respective results, only noise and signal power situated within the respective sub-band are taken into account. In this case (11) describes the *SNR* scaling for a specific sub-band of width $B_{sub}$ around a center frequency $f_c$. In both cases, if multiple bursts are considered, the respective signal and noise powers have to be added before the sums are related.

$$\Phi_{bf1,B,i}\left(PRF, f_{c,t}\right) = \frac{p_{n,el} \cdot \sum_{j=1}^{N} \mathrm{E}\left[\left|P_{j,PRF}\left(f\right)\right|^2 \cdot rect\left(f/B_D\right)\right]}{N \cdot \mathrm{E}\left[\left|U\left(f\right) \cdot W\left(B_{s,i}\right)\right|^2\right]} \tag{10}$$

$$\Phi_{bf2,B}\left(PRF, f_{c,t}\right) = \frac{p_{n,el} \cdot \sum_{j=1}^{N} \mathrm{E}\left[\left|P_{j,PRF}\left(f\right)\right|^2 \cdot rect\left(\frac{f-f_c}{B_{sub}}\right)\right]}{N \cdot \mathrm{E}\left[\left|U\left(f\right) \cdot rect\left(\frac{f-f_c}{B_{sub}}\right)\right|^2\right]} \tag{11}$$

## 3. ScanSAR System Design Example

### 3.1 Timing and System Parameter

In the following, an X-band system with the requirements and system constraints as summarized by Table 1 is designed. In a first step, a timing analysis is performed yielding the following result to cover a swath of 400 km by 4 sub-swaths of length 105 km each with an orbit height of 630 km (cf. Fig. 4). The necessary *PRFs* vary only from 1150 Hz up to 1240 Hz, what is a quite good-natured case. If a larger *PRF* range is needed, e.g. caused by orbit height variations, optimization strategies as presented in [1] will become necessary.

| Parameter | Symbol | Value |
|---|---|---|
| Carrier wavelength | $\lambda$ | 3.1 cm |
| Swath-width on ground | $W_g$ | ≥ 400 km |
| Geometric resolution in azimuth | $\delta_{az}$ | ≤ 5 m |
| Azimuth ambiguity suppression | $AASR_{N,B}$ | ≤ -20 dB |
| Covered incident angle range | $\Theta_i$ | 19 - 47° |
| Transmit duty cycle | $dc$ | 15 % |

**TABLE 1. Requirements and system constraints.**

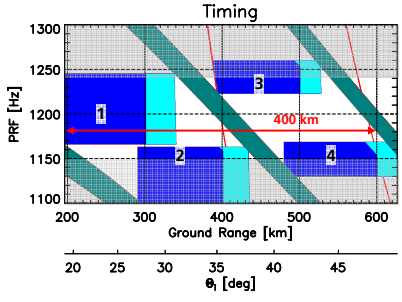


**Fig. 4. Timing diagram considering transmit events (green) and nadir returns (red). 4 swaths of length 105 km each cover a ground range of 400 km.**

In order to ensure a $PRF_{uni}$ situated within the *PRF* range of operation, the overall length of the antenna has to be adapted. We choose 12.6 m yielding a $PRF_{uni}$ of ~1200 Hz. Further, the necessary bandwidth of a single burst is chosen to 1.25 kHz to achieve a resolution of 5 m if a single burst is processed. This yields a system bandwidth $B_D$=*6.25 kHz* (cf. (6)). In combination with the minimum *PRF*, this would require a minimum number of *6* receive apertures to fulfil the Nyquist criterion according to (12). Nevertheless, *N=7* is chosen to better adapt the single receive aperture size to $B_D$ and to guarantee a sufficient oversampling.

$$N \geq \frac{B_D}{PRF_{min}} \tag{12}$$

Finally, the transmit antenna length in azimuth is set to 2.8 m, what is large enough to ensure sufficient ambiguity suppression but small enough to obtain a resolution of 5 m. All parameters are summarized in Table 2.

| Parameter | Symbol | Value |
|---|---|---|
| Orbit height | $h_s$ | 630 km |
| Sensor velocity | $v_s$ | 7545 m/s |
| *PRF* range of operation | *PRF* | 1150 - 1240 Hz |
| Subswath-width on ground | $W_{g,s}$ | 105 km |
| No. of subswaths/bursts | $N_B$ | 4 |
| Rx sub-apertures in azimuth | $N$ | 7 |
| Rx sub-aperture length in azimuth | $d_{a,rx}$ | 1.8 m |
| Tx antenna length in azimuth | $d_{a,tx}$ | 2.8 m |
| Cycle time | $T_C$ | 1.12 s |
| Burst duration | $T_B$ | 0.28 s |
| Burst bandwidth | $B_B$ | 1.25 kHz |
| Processed azimuth bandwidth | $B_D$ | 6.25 kHz |

**TABLE 2. System parameters.**

### 3.2 Performance Analysis

#### 3.2.1 Geometric Resolution in Azimuth: $\delta_{az}$

The geometric resolution is constant over the *PRF* but varies depending on $f_{c,t}$. If a single burst is processed, a resolution better than 5 m is achieved with a slight decrease from 4.9 m up to 5 m for increasing $f_{c,t}$. For the addition of two bursts a resolution from 4.9 m for centered targets up to 5.6 m for targets located closer to the egdes of the burst (dashed blue line) is obtained.

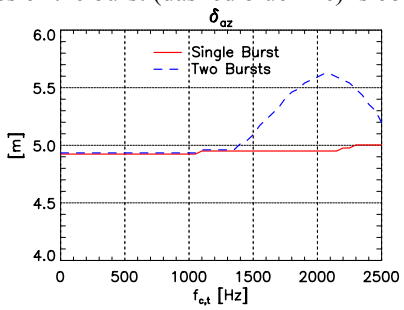


**Fig. 5. Resolution in azimuth ($\delta_{az}$) vs. $f_{c,t}$ for one burst (solid red) and the addition of two bursts (dashed blue).**

### 3.2.2 Azimuth-Ambiguity-to-Signal Ratio: $AASR_{N,B}$

Fig. 6 and Fig. 7 show the $AASR_{N,B}$ in dependency of *PRF* and $f_{c,t}$ for the processing of a single burst and the addition of two bursts, respectively. In the considered *PRF* range the $AASR_{N,B}$ is below the required -20 dB.

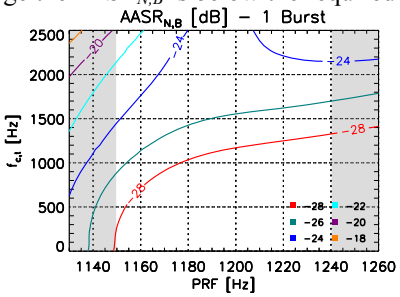


**Fig. 6. Ambiguous Energy Suppression ($AASR_{N,B}$) for a single burst vs. *PRF* and $f_{c,t}$.**

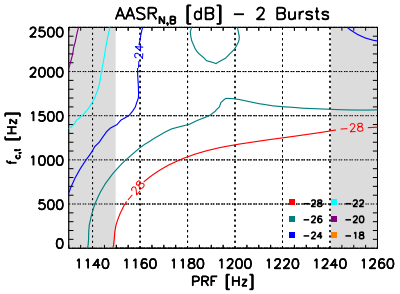


**Fig. 7. Ambiguous Energy Suppression ($AASR_{N,B}$) for two added bursts vs. *PRF* and $f_{c,t}$.**

### 3.2.3 *SNR* Scaling Factor: $\Phi_{bf,B}$

Firstly, consider the case where the complete band $B_D$ is focused (cf. 2.3). Then the *SNR* scaling for targets situated at $f_{c,t}=0$ corresponds to the $\Phi_{bf}$ of a stripmap system given in Fig. 8. One observes a nearly negligible maximum degradation of 0.13 dB due to the processing. Further, Fig. 9 gives the ScanSAR-inherent loss of the signal power in dependency on the target position and related to the value at $f_{c,t}=0$. This scalloping

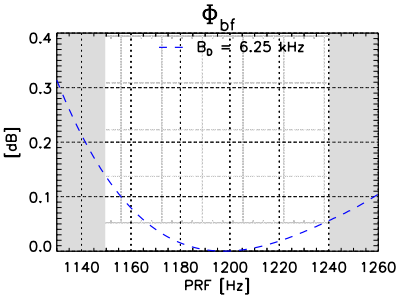


**Fig. 8. *SNR* scaling factor ($\Phi_{bf}$) vs. *PRF*.**

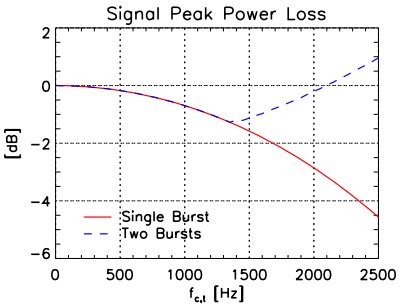


**Fig. 9. Signal peak power loss vs. $f_{c,t}$ for a single burst (solid red) and the addition of two bursts (dashed blue).**

shows a maximum decrease of the signal power by ~1.25 dB if two bursts are added while a loss of up to ~4.5 dB is encountered for a single burst. The burst mode *SNR* scaling factor $\Phi_{bf,B}$ is then obtained by combining $\Phi_{bf}$ of Fig. 8 and the scalloping of Fig. 9.

Secondly, multiple separate sub-bands are focused and (11) becomes valid to describe the *SNR* within one of these sub-bands. In contrast to the case mentioned above, now the scaling of the noise power also depends on the center frequency $f_c$ of the focused band entailing a scalloping-like effect. In the present case - and with $B_{sub}=B_B$, $f_c = f_{c,t}$ - this yields an uncritical maximum degradation of 0.17 dB. The scalloping of the signal power stays the same as above (cf. Fig. 9).

## 4. Summary

In the frame of advanced concepts for ultra-wide-swath SAR imaging [2] a multi-channel ScanSAR system design example demonstrated the applicability of multi-aperture signal processing in burst mode operation. This enabled the imaging of an ultra-wide-swath of 400 km with a geometric resolution of 5 m. Further, the analytic descriptions of performance parameters like azimuth ambiguous energy suppression ($AASR_N$) and *SNR* and how they are affected by the digital processing network were extended to burst mode operation. In this context a scalloping-like effect for azimuth ambiguities depending on the target position within the burst was described that is caused by the Doppler frequency dependent weighting of the beamforming network. A possible rise of the noise power depends on the focusing method that can either entail a stripmap-like behaviour or a scalloping-like variation, while the signal power always varies with the target position within the burst. A consideration of both effects then allows for determining the *SNR*.

The ScanSAR system was chosen exemplarily to demonstrate the potential of ultra-wide-swath imaging with burst modes. The derived results can be transferred to TOPS SAR or innovative concepts as the multi-beam burst mode (MBBM) system that is based on multiple transmit beams enabling the simultaneous acquisition of multiple sub-swaths within the same burst [2].

## References


[1] N. Gebert, G. Krieger, A. Moreira, "Digital Beamforming on Receive: Techniques and Optimization Strategies for High-Resolution Wide-Swath SAR Imaging", *IEEE Trans. Aerospace and Electronic Systems*, accepted for publication.

[2] G. Krieger, et al., „Advanced Concepts for Ultra-Wide-Swath SAR Imaging with High Azimuth Resolution", *Proceedings of EUSAR*, Friedrichshafen, Germany, 2008.

[3] K. Tomiyasu, "Conceptual performance of a satellite borne, wide swath synthetic aperture radar", *IEEE Trans. Geoscience and Remote Sensing*, vol. 19, pp. 108-116, 1981.

[4] R. K. Moore, J. P. Claassen, Y. H. Lin, "Scanning spaceborne synthetic aperture radar with integrated radiometer", *IEEE Trans. Aerospace and Electronic Systems*, vol. 17, pp. 410-421, 1981.

[5] F. De Zan, A.M. Monti Guarnieri, "TOPSAR: Terrain Observation by Progressive Scans", *IEEE Trans. Geoscience and Remote Sensing*, vol. 44, pp. 2352 – 2360, 2006.